Reduction of IBR-dominated Distribution Networks by Multi-port Synthesis and Clustering

D. del Giudice*, S. Haddadi Vaighan*, F. Bizzarri*, D. Linaro*, A.M. Brambilla*
* Department of Electronics, Information Technology and Bioengineering, Politecnico di Milano, Milan, Italy.
Email: {name.surname@polimi.it}

***Abstract*—A challenge posed by the increasing penetration of inverter-based resources (IBRs) in distribution networks is how to efficiently simulate a transmission system with a large number of them, since this leads to an "explosion" in system complexity. This paper presents a two-step reduction method for IBR-dominated distribution networks. In the first step, the approach synthesizes a distribution network as a multi-port: one port at the substation connecting it to the transmission system and the others for each IBR connected to the feeder. Then, in the second step, IBRs at the connecting ports are possibly clustered, thus reducing their number. The method differs from others in the literature since it is *numerical* and can handle clusters of IBRs with different power ratings and set-points. Simulation results of a distribution network with IBRs show the effectiveness of the method.**

I. Introduction

Over the last years, distribution networks (i.e., feeders) have witnessed an ever-increasing penetration of inverter-based resources (IBRs), given for example by renewable energy sources (RESs) at domestic utilities. This trend affects not only the way electric power systems are planned and operated, but also how they are analyzed and simulated [1]. Power system simulation is a crucial tool transmission system operators exploit to ensure network stability in a wide range of operating conditions. Before the significant increase in IBR penetration, a common simulation approach consisted in replacing each feeder with *a single* equivalent load at the substation connecting the feeder to the transmission system [2]. Albeit efficient in reducing the computational cost needed to simulate large-scale power systems with many feeders, this practice was effective since feeders were *passive*, that is, they were almost entirely made up of (non)-linear loads. However, this assumption is violated by the recently rising share of IBRs, which is turning distribution feeders into *active* networks, whose dynamics cannot be captured by conventional (non)-linear load models [3].

In this context, the main solutions proposed in the literature to develop possibly active distribution network equivalents (DNEs) can be divided into two main groups: *measurement-based* and *model-based*. Measurement-based approaches rely on active and reactive power exchange responses at the substation during different voltage disturbances, which are either caused by real events and recorded or artificially introduced through simulations [5], [6]. After choosing a DNE model (see for example [7]), its parameters are fitted to match these responses. Though straightforward to implement, these approaches require the availability of many responses to prevent over-fitting and ensure adequate DNE generalization.

The work of Federico Bizzarri was partially supported by Italian MUR under Grant PRIN 2022 DCNanoSyn, CUP D53D23001500006, Project Code 2022SPFP9R.

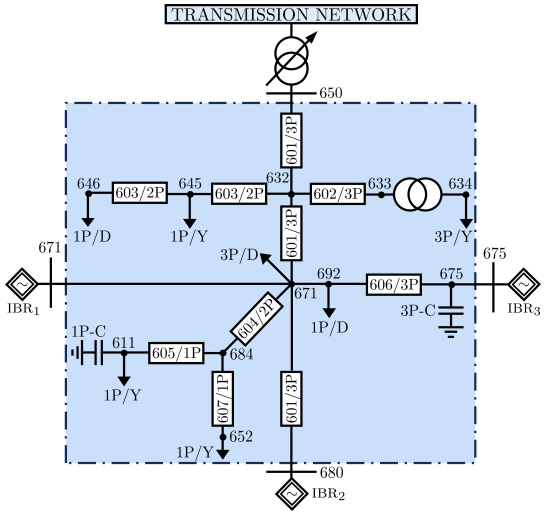

Fig. 1. The schematic of the IEEE13 bus feeder, modified by adding three IBRs. Feeder data, including cable/load types and phases, is reported in [4].

Model-based approaches hinge on the knowledge of the feeder models. This, together with the power flow solution (PFS) of the system (corresponding to its steady-state operating point), is exploited to obtain a compact DNE, where as many IBRs as possible are grouped into a single representative (clustered) and simulated as a single equivalent entity [8]–[10]. For example, in [9] if the equivalent impedances "seen" from the substation toward a set of IBR buses are similar, then these IBRs are considered belonging to the same cluster. This criterion stems from the fact that these impedances mirror the voltage sensitivities of IBRs, which indicate how their power exchange varies with the voltage at each bus connecting an IBR to the feeder. If IBRs have a similar voltage sensitivity, then they will react analogously to a disturbance in the transmission network and, thus, can be clustered.

In [10], the equivalent is built *analytically* from the IBR model equations. Contrary to [9], [10] specifies how to cluster IBRs, possibly with different power ratings and set-points. However, this quickly becomes cumbersome if the IBR model changes or is complex, as the necessary pen-and-paper calculations for clustering must be repeated from scratch.

Here, we propose a completely *numerical*, two-step method for deriving DNEs. At first, the feeder is reduced and synthe-

sized as a multi-port, whose ports are that at the substation connecting it to the transmission system and the others at the buses connecting each IBR to the feeder. A second step further reduces the size of the multi-port, by grouping as many IBRs as possible in clusters. Each cluster, potentially including IBRs of different power ratings and set-points, is thus reduced to a single IBR. A benchmark feeder is used as a means to describe the proposed approach and highlight its performance.

II. DNE DERIVATION

We selected the IEEE13 bus feeder in Fig. 1 (modified by adding three IBRs) as a test platform to introduce in the simplest terms the two steps of the proposed method.

A. First step: multi-port synthesis of a feeder

In the first step, the power flow solution (PFS) of the feeder is computed. At the PFS, its linear model is represented as a hybrid multi-port given by

$$\underbrace{\begin{bmatrix}\boldsymbol{\imath_{650}}\\ \boldsymbol{v_{671}}\\ \boldsymbol{v_{675}}\\ \boldsymbol{v_{680}}\end{bmatrix}}_{\boldsymbol{\alpha}} = \boldsymbol{H}\underbrace{\begin{bmatrix}\boldsymbol{v_{650}}\\ \boldsymbol{\imath_{671}}\\ \boldsymbol{\imath_{675}}\\ \boldsymbol{\imath_{680}}\end{bmatrix}}_{\boldsymbol{\beta}} + \underbrace{\begin{bmatrix}\boldsymbol{\imath}^{\text{PF}}_{\boldsymbol{650}}\\ \boldsymbol{v}^{\text{PF}}_{\boldsymbol{671}}\\ \boldsymbol{v}^{\text{PF}}_{\boldsymbol{675}}\\ \boldsymbol{v}^{\text{PF}}_{\boldsymbol{680}}\end{bmatrix} - \boldsymbol{H}\begin{bmatrix}\boldsymbol{v}^{\text{PF}}_{\boldsymbol{650}}\\ \boldsymbol{\imath}^{\text{PF}}_{\boldsymbol{671}}\\ \boldsymbol{\imath}^{\text{PF}}_{\boldsymbol{675}}\\ \boldsymbol{\imath}^{\text{PF}}_{\boldsymbol{680}}\end{bmatrix}}_{\boldsymbol{J}}, \quad (1)$$

where $\boldsymbol{\alpha}$ and $\boldsymbol{\beta}$ are the outputs and inputs, respectively, and the $^{\text{PF}}$ superscript refers to the PFS. Equation (1) retains only the ports associated to the transmission network (bus 650) and IBRs (buses 671, 675, and 680), which are voltage and current-driven, respectively. Each port variable is written in bold to indicate that they are vectors (e.g., $\boldsymbol{\imath_{650}} = [\imath_{650_a}, \imath_{650_b}, \imath_{650_c}]^T$), that is, $\boldsymbol{\imath_{650}}$ includes the current in each phase at bus 650; thus, each port may be *multi-phase*. To derive this formulation, it is necessary (i) to replace the feeder's internal loads with equivalent admittances and (ii) to compute the hybrid matrix $\boldsymbol{H}$, as $\boldsymbol{J}$ can be derived knowing $\boldsymbol{H}$ and the PFS.

The feeder in Fig. 1 is synthesized as in Fig. 2(a) after the first step. Compared to the original network, the computational cost associated to the simulation of the DNE is generally lower (especially in large-scale feeders) because it retains fewer nodes, elements, and, thus, electrical variables. However, if the network under study includes many IBRs, the reduction in CPU time granted by the first step may be insufficient, as it includes a port for each IBR. This issue is addressed with the second step, which clusters as many IBRs as possible and represents them with a single representative IBR per cluster.

B. Second step: IBR clustering and DNE reduction

To cluster IBRs, we rely on the following steps.

1) Compute $\boldsymbol{P} = (\boldsymbol{H} \odot \boldsymbol{\beta})^{|\cdot|}$ (i.e., the absolute value of the element-wise product of $\boldsymbol{H}$ and $\boldsymbol{\beta}$) at the PFS.
2) Divide each entry of $\boldsymbol{P}$ by its respective row sum, obtaining the matrix $\boldsymbol{W}$ of per-unit weights.
3) Re-shape and re-organize $\boldsymbol{W}$ so that its diagonal elements are moved in a new column and the original entries are replaced by zeros.
4) IBRs are clustered if their models are the same and the absolute value of the difference between their corresponding rows in $\boldsymbol{W}$ is lower than a threshold ε, chosen heuristically.

After identifying those IBRs that can be clustered, they are grouped and only a representative one is simulated, thus obtaining a *reduced* DNE that includes as ports the transmission network and the representative IBRs only (i.e., one per cluster). To explain how this reduction works, consider as an example the case where IBR_2 needs to be simulated separately, while IBR_1 and IBR_3 in Fig. 2(a) can be clustered (with the former picked as representative). The reduced DNE is shown in Fig. 2(b) and is described as

$$\underbrace{\begin{bmatrix}\boldsymbol{\imath_{650}}\\ \boldsymbol{v_{671}}\\ \boldsymbol{v_{680}}\end{bmatrix}}_{\boldsymbol{\alpha_r}} = \boldsymbol{H_r}\underbrace{\begin{bmatrix}\boldsymbol{v_{650}}\\ \boldsymbol{\imath_{671}}\\ \boldsymbol{\imath_{680}}\end{bmatrix}}_{\boldsymbol{\beta_r}} + \boldsymbol{J_r}\,, \quad (2)$$

where the $_r$ subscript is used to denote the variables of the *reduced* DNE. To show how $\boldsymbol{H_r}$ and $\boldsymbol{J_r}$ can be derived, we introduce the $\boldsymbol{T_A}$, $\boldsymbol{T_B}$ matrices and $\boldsymbol{T_C}$ vector. $\boldsymbol{T_A}$ links the outputs of the reduced and unreduced DNEs $\boldsymbol{\alpha_r}$ and $\boldsymbol{\alpha}$ as

$$\underbrace{\begin{bmatrix}\boldsymbol{\imath_{650}}\\ \boldsymbol{v_{671}}\\ \boldsymbol{v_{680}}\end{bmatrix}}_{\boldsymbol{\alpha_r}} = \underbrace{\begin{bmatrix}\mathbb{1}_k & \mathbb{0}_k & \mathbb{0}_k & \mathbb{0}_k\\ \mathbb{0}_k & \mathbb{1}_k & \mathbb{0}_k & \mathbb{0}_k\\ \mathbb{0}_k & \mathbb{0}_k & \mathbb{0}_k & \mathbb{1}_k\end{bmatrix}}_{\boldsymbol{T_A}} \underbrace{\begin{bmatrix}\boldsymbol{\imath_{650}}\\ \boldsymbol{v_{671}}\\ \boldsymbol{v_{675}}\\ \boldsymbol{v_{680}}\end{bmatrix}}_{\boldsymbol{\alpha}}, \quad (3)$$

with $\mathbb{1}_k$ and $\mathbb{0}_k$ being $k\times k$ identity and null matrices, respectively, which are suitably inserted in $\boldsymbol{T_A}$ to ensure the outputs of the aggregated IBRs (i.e., $\boldsymbol{v_{675}}$ in this case) do not matter in the computation of the reduced output vector $\boldsymbol{\alpha_r}$[1].

$\boldsymbol{T_B}$ and $\boldsymbol{T_C}$ relate the inputs of the unreduced and reduced DNEs $\boldsymbol{\beta}$ and $\boldsymbol{\beta_r}$ as follows:

$$\underbrace{\begin{bmatrix}\boldsymbol{v_{650}}\\ \boldsymbol{\imath_{671}}\\ \boldsymbol{\imath_{675}}\\ \boldsymbol{\imath_{680}}\end{bmatrix}}_{\boldsymbol{\beta}} = \underbrace{\begin{bmatrix}\mathbb{1}_k & \mathbb{0}_k & \mathbb{0}_k\\ \mathbb{0}_k & \mathbb{1}_k & \mathbb{0}_k\\ \mathbb{0}_k & \boldsymbol{\gamma} & \mathbb{0}_k\\ \mathbb{0}_k & \mathbb{0}_k & \mathbb{1}_k\end{bmatrix}}_{\boldsymbol{T_B}} \underbrace{\begin{bmatrix}\boldsymbol{v_{650}}\\ \boldsymbol{\imath_{671}}\\ \boldsymbol{\imath_{680}}\end{bmatrix}}_{\boldsymbol{\beta_r}} + \underbrace{\begin{bmatrix}\mathbb{0}_{k,1}\\ \mathbb{0}_{k,1}\\ \boldsymbol{\eta}\\ \mathbb{0}_{k,1}\end{bmatrix}}_{\boldsymbol{T_C}}, \quad (4)$$

where $\mathbb{0}_{k,1}$ is a vector of zeros with k entries. As for $\boldsymbol{T_B}$, the insertion of $\mathbb{1}_k$ and $\mathbb{0}_k$ in the rows of the retained ports ($\boldsymbol{v_{650}}$,

[1] If the transmission grid and all IBRs are three-phase, then $k = 3$. Here we considered this case to keep notation terse. However, the formulation is easily adaptable to grids with a neutral wire, and single and three-phase IBRs.

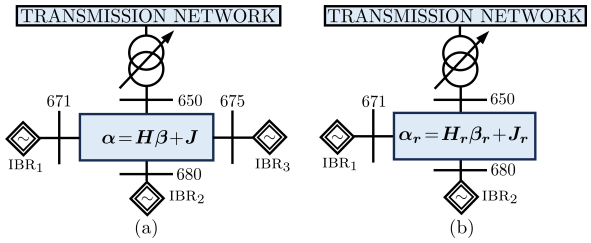

Fig. 2. Unreduced (a) and reduced (b) DNE of the IEEE13 bus feeder in Fig. 1 obtained after the first and second step of the proposed method (assuming IBR_1 and IBR_3 can be clustered and represented through the former).

$\boldsymbol{\imath_{671}}$, and $\boldsymbol{\imath_{680}}$ in this case) is analogue to that used to build $\boldsymbol{T_A}$. On the contrary, the rows of the input associated with the clustered IBRs ($\boldsymbol{\imath_{675}}$) are exclusively related to those of the representative IBR ($\boldsymbol{\imath_{671}}$) through a block diagonal matrix $\boldsymbol{\gamma}$. On the contrary, the vector $\boldsymbol{T_C}$ contains zeros except for the rows of the clustered IBRs, where a vector $\boldsymbol{\eta}$ is introduced.

To detail how $\boldsymbol{\gamma}$ and $\boldsymbol{\eta}$ are derived, we focus on the row $\imath_{675_a}$ of $\boldsymbol{\imath_{675}}$ and on the homologous variable of the representative IBR $\imath_{671_a}$. DNEs should replicate the behavior of their original counterparts during disturbances in the transmission network (bus 650 in Fig. 1). For example, if a small voltage disturbance Δv_{650_a} occurs at phase a of bus 650 (probing signal), the small-signal response of currents $\imath_{671_a}$ and $\imath_{675_a}$ is

$$\begin{aligned} \Delta\imath_{671_a} &= \imath_{671_a} - \imath^{\text{PF}}_{671_a} = \mathcal{L}^{-1}\{f_1(s)\Delta v_{650_a}(s)\} \\ \Delta\imath_{675_a} &= \imath_{675_a} - \imath^{\text{PF}}_{675_a} = \mathcal{L}^{-1}\{f_2(s)\Delta v_{650_a}(s)\}\,, \end{aligned} \tag{5}$$

where $\mathcal{L}^{-1}$ is the inverse Laplace transform operator. $f_1(s)$ and $f_2(s)$ are computed by the AC analysis available in circuit simulators, and are used to derive the entries of $\boldsymbol{\gamma}$ and $\boldsymbol{\eta}$.
To better describe this, let us identify two cases. First, IBR_1 and IBR_3 have the same power rating, set-point, and can be clustered; at the PFS their operating points are almost the same and the same holds for their responses to external voltage disturbances[2]. Thus, $\imath^{\text{PF}}_{675_a} \approx \imath^{\text{PF}}_{671_a}$ and $f_2(s) \approx f_1(s)$ across the whole frequency range and

$$\frac{\Delta\imath_{675_a}}{\Delta\imath_{671_a}} = \frac{\mathcal{L}^{-1}\{f_2(s)\Delta v_{650_a}(s)\}}{\mathcal{L}^{-1}\{f_1(s)\Delta v_{650_a}(s)\}} \approx 1\,. \tag{6}$$

Hence, using (5) and (6), $\imath_{675_a}$ can be rewritten as

$$\begin{aligned} \imath_{675_a} &= \imath^{\text{PF}}_{675_a} + \Delta\imath_{675_a} \approx \imath^{\text{PF}}_{675_a} + \Delta\imath_{671_a} \\ &= \underbrace{1}_{\gamma_{1,1}} \cdot \imath_{671_a} + \underbrace{\left(\imath^{\text{PF}}_{675_a} - \imath^{\text{PF}}_{671_a}\right)}_{\eta_1}{}^{\to 0}\,. \end{aligned} \tag{7}$$

In general, the two IBRs may have different power ratings and set-points. If so, the ratio in (6) is not approximately equal to 1. Therefore, $f_1(s)$ and $f_2(s)$ are analyzed only at low frequency (e.g., 10 mHz), where they are almost constant and real (i.e., the ratio in (6) can be approximated by $\chi \in \mathbb{R}$). This choice introduces an error in the high-frequency response of the DNE to disturbances but limits its complexity.
With these assumptions, $\imath_{675_a}$ can be recast as

$$\begin{aligned} \imath_{675_a} &= \imath^{\text{PF}}_{675_a} + \Delta\imath_{675_a} \approx \imath^{\text{PF}}_{675_a} + \chi\Delta\imath_{671_a} \\ &= \underbrace{\chi}_{\gamma_{1,1}} \cdot \imath_{671_a} + \underbrace{\left(\imath^{\text{PF}}_{675_a} - \chi\imath^{\text{PF}}_{671_a}\right)}_{\eta_1}\,. \end{aligned} \tag{8}$$

Equations (7) and (8) show how a generic entry of $\boldsymbol{\gamma}$ and $\boldsymbol{\eta}$ is derived. To compute the whole matrix and vector, this procedure is repeated for each phase of the clustered IBRs. Based on (1), (3), and (4), the reduced DNE formulation in (2) can be finally derived as

$$\begin{aligned} \boldsymbol{\alpha_r} &= \boldsymbol{T_A}\boldsymbol{\alpha} = \boldsymbol{T_A}\left(\boldsymbol{H}\boldsymbol{\beta} + \boldsymbol{J}\right) \\ &= \boldsymbol{T_A}\left(\boldsymbol{H}\left(\boldsymbol{T_B}\boldsymbol{\beta_r} + \boldsymbol{T_C}\right) + \boldsymbol{J}\right) \\ &= \underbrace{\boldsymbol{T_A}\boldsymbol{H}\boldsymbol{T_B}}_{\boldsymbol{H_r}}\boldsymbol{\beta_r} + \underbrace{\boldsymbol{T_A}\left(\boldsymbol{H}\boldsymbol{T_C} + \boldsymbol{J}\right)}_{\boldsymbol{J_r}}\,. \end{aligned} \tag{9}$$

[2]The term *almost* is used as clustering is done based on the tolerance ε.

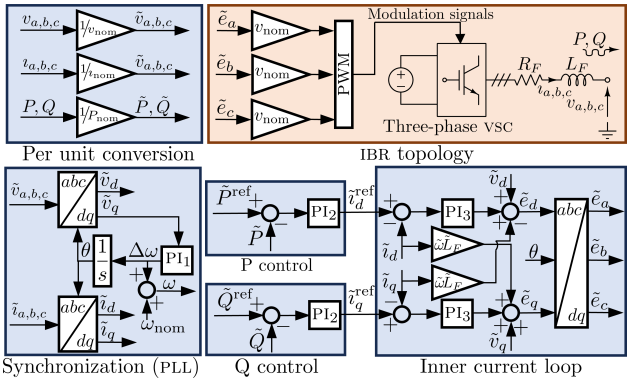

Fig. 3. Topology and control scheme of the IBR adopted in this work, which is a simplification of that in [14].

As a consequence, after identifying those IBRs that can be clustered, the derivation of the reduced DNE (i.e., $\boldsymbol{H_r}$ and $\boldsymbol{J_r}$) requires building and then exploiting $\boldsymbol{T_A}$, $\boldsymbol{T_B}$, and $\boldsymbol{T_C}$.[3] These tasks, along with those needed in the first step of the proposed method, can be implemented in a simulator to reduce feeders of any kind and size with any number of IBRs.

III. Simulation Results

To show the effectiveness of the proposed method, we tested it to synthesize and reduce the modified IEEE13 feeder in Fig. 1 in two different cases. In both cases, a voltage step of 10% applied at 0.25 s at the feeder substation was simulated to test if the dynamics of the DNE obtained through the proposed method matched those of the original network. Simulations were performed with PAN [11]–[13] on an INTEL® Xeon® GOLD-6238R-CPU@2.20 GHz, running LINUX MINT 20.1.

We adopted the IBR model sketched in Fig. 3. Hereafter we describe only the key features necessary for understanding the following simulation results (we refer the interested reader to [14] for details on the IBR control scheme). In a nutshell, the converter is of *grid-following* kind; it regulates the amplitude and phase of its voltage source to ensure the exchanged active and reactive powers (P and Q) match the reference value (set-point), denoted by the $^{\text{ref}}$ superscript. The set-points either derive from other controls (e.g., frequency and voltage droop) or can be fixed values, as assumed for simplicity in this work. All the measurements and control blocks are formulated in per-unit, denoted by the $\tilde{}$ symbol: in other words, all variables are normalized to a base value (e.g., v_{nom}, $\imath_{\text{nom}}$, and P_{nom}). This allows flexible re-usage of the same IBR model in several different instances with different voltage and power ratings.

In the first simulation case, all IBRs have the same power rating ($P_{\text{nom}} = 3500$ kW) and per-unit set-points ($\tilde{P}^{\text{ref}} = 1$ and $\tilde{Q}^{\text{ref}} = 0.2$). In addition, the length of the line between buses 671 and 680 is increased tenfold with respect to its default value in [4] to force the exclusion of IBR_2 from IBR clustering with reasonable ε values. This action changes the equivalent impedance between the feeder substation and IBR_2 and thus its voltage sensitivity with respect to the other IBRs.

[3]If the ratio in (6) was analyzed over the *whole* frequency range, χ would be complex and frequency-dependent rather than real and constant. This would result in a more computationally intensive and complex formulation of (9).

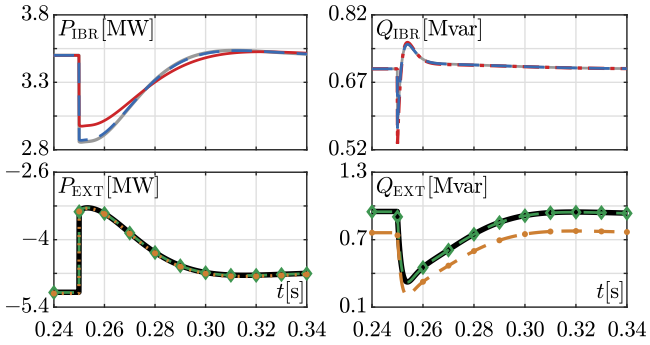

Fig. 4. Simulation results of the modified IEEE13 bus feeder obtained in the first case. Refer to the main text for the description of the case, as well as the color code and meaning of each trace. Top panels: active (left) and reactive (right) power of each IBR in the original network. Bottom panels: active (left) and reactive (right) power exchange at the feeder substation in the original network and in the DNE for different values of clustering tolerance ε.

Figure 4 depicts the obtained results. The top panels show the P_{IBR} and Q_{IBR} active and reactive power exchange of IBR_1, IBR_2, and IBR_3 (**gray**, **red**, and **blue** traces, respectively). As expected, the impact of the different voltage sensitivity of IBR_2 is evident, especially in the top left panel, where the active power exchange of IBR_2 after the voltage disturbance is visibly different from that of the other IBRs.

These results suggest that ε should be chosen so that the derived DNE simulates IBR_2 separately, while IBR_1 and IBR_3 can be grouped and represented for example by the former (i.e., the same scenario used to describe the operating principle of the method in Section II-B). The bottom panels of Fig. 4 show the active and reactive powers P_{EXT} and Q_{EXT} at the feeder substation (bus 650) in three scenarios. The **black** trace refers to the results of the original network, while the **green** and **orange** traces refer to the results obtained by the DNE when ε is equal to 0.1 and 0.5, respectively. When $\varepsilon = 0.1$, IBR_2 is not clustered with the other IBRs and, as expected, the results well match those of the original network. When $\varepsilon = 0.5$, all IBRs are clustered: despite leading to a more compact DNE, errors are introduced, as shown in the middle right panel. Thus, the selection of tolerance ε derives from trade-off between DNE accuracy and speed: the fewer the retained IBRs, the faster the simulation of the DNE, but the lower its accuracy.

In the second simulation case, we restored the original line length between buses 671 and 680, set the per-unit power set-point of IBR_2 at 0.8 and the rating of IBR_3 at 1400 kW. So doing, we simulate a case where IBRs have different power ratings and/or set-points. With $\varepsilon = 0.1$, all IBRs are clustered and IBR_1 is chosen as the representative one. Figure 5 shows the results of this case. The top panels highlight how P_{IBR} and Q_{IBR} of each IBR change with P_{nom} and $\widetilde{P}^{\text{ref}}$, while the middle panels compare P_{EXT} and Q_{EXT} in the original and reduced systems. The comparison highlights how the reduction method retains a high accuracy when simulating external voltage disturbances. The dashed area in the middle right panel indicates that there is just a slight mismatch between the results of the DNE (**green** trace) and the original network (**black** trace) right after the voltage disturbance. Differences

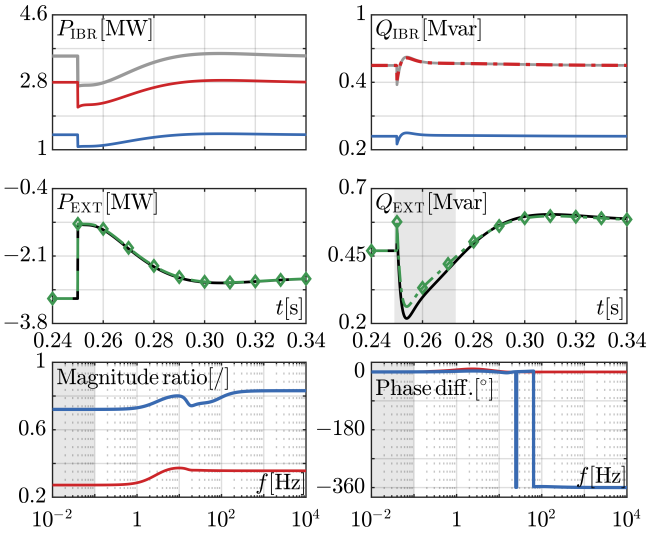

Fig. 5. Simulation results of the modified IEEE13 bus feeder obtained in the second case. Refer to the main text for the description of the case, as well as the color code and meaning of each trace. The top and middle panels are analogous to those of Fig. 4. The bottom panels show the magnitude ratio (left) and phase difference (right) between v_{675_a} and v_{671_a} and that between v_{680_a} and v_{671_a}, obtained through AC analysis.

can be justified by looking at the bottom panels, which show the magnitude of the ratio and phase difference between v_{675_a} and v_{671_a} (**red** trace) and that between v_{680_a} and v_{671_a} (**blue** trace), both obtained by an AC analysis through the injection of a small voltage disturbance at bus 650 (phase a). These variables are used to derive the entries of $\boldsymbol{\gamma}$ and $\boldsymbol{\eta}$ using (7) and (8). As stated in Section II-B, they are computed by looking at the χ ratio between transfer functions at low frequency (shaded areas in the bottom panels) and assuming it fixed in the entire frequency range. However, this ratio actually evolves with frequency and by considering it fixed, the high-frequency dynamics of each IBR is not captured, introducing differences in Q_{EXT} *right after* the voltage disturbance. This way of computing χ is chosen to limit the complexity of the DNE as it leads to slight differences in the simulation results.

Lastly, it is worth noting that the CPU time needed to simulate the DNE in the time-domain is 33% less than that of the original network: we expect this efficiency gain to increase further when the method is applied to large-scale feeders.

IV. Conclusions

In this work, we proposed a method for reducing distribution networks (feeders) through multi-port synthesis and IBR clustering. We purposely chose as a benchmark a relatively small system to explain the method in its simplest terms. Nevertheless, it can be applied to distribution networks of any size, be they balanced or unbalanced, which also include IBRs different from those in Fig. 3 and that are three-phase or single-phase. Future work will be devoted to show the effectiveness of the method in such cases, which have been preliminarily tested but could not be shown here for space reasons.

REFERENCES

[1] J. Matevosyan, J. MacDowell, N. Miller, B. Badrzadeh, D. Ramasubramanian, A. Isaacs, R. Quint, E. Quitmann, R. Pfeiffer, H. Urdal, T. Prevost, V. Vittal, D. Woodford, S. H. Huang, and J. O'Sullivan, "A future with inverter-based resources: Finding strength from traditional weakness," *IEEE Power and Energy Magazine*, vol. 19, no. 6, pp. 18–28, 2021.

[2] J. V. Milanović, K. Yamashita, S. Martínez Villanueva, S. Z. Djokic, and L. M. Korunović, "International industry practice on power system load modeling," *IEEE Transactions on Power Systems*, vol. 28, no. 3, pp. 3038–3046, 2013.

[3] D. del Giudice, F. Bizzarri, S. Grillo, D. Linaro, and A. M. Brambilla, "Impact of passive-components' models on the stability assessment of inverter-dominated power grids," *Energies*, vol. 15, no. 17, 2022.

[4] W. Kersting, "Radial distribution test feeders," in *2001 IEEE Power Engineering Society Winter Meeting. Conference Proceedings (Cat. No.01CH37194)*, vol. 2, 2001, pp. 908–912 vol.2.

[5] Y. Zhu and J. V. Milanović, "Automatic identification of power system load models based on field measurements," *IEEE Transactions on Power Systems*, vol. 33, no. 3, pp. 3162–3171, 2018.

[6] G. Chaspierre, G. Denis, P. Panciatici, and T. Van Cutsem, "A dynamic equivalent of active distribution network: Derivation, update, validation and use cases," *IEEE Open Access Journal of Power and Energy*, vol. 8, pp. 497–509, 2021.

[7] G. A. Barzegkar-Ntovom, E. O. Kontis, T. A. Papadopoulos, and P. N. Papadopoulos, "Methodology for evaluating equivalent models for the dynamic analysis of power systems," *IEEE Transactions on Power Delivery*, vol. 37, no. 6, pp. 5059–5070, 2022.

[8] J. Ungerland, N. Poshiya, W. Biener, and H. Lens, "A voltage sensitivity based equivalent for active distribution networks containing grid forming converters," *IEEE Transactions on Smart Grid*, vol. 14, no. 4, pp. 2825–2836, 2023.

[9] J. Ungerland and H. Lens, "Evaluation of equivalent dynamic active distribution network models with individual and aggregated consideration of grid forming converters," *Energy Technology*, vol. 11, no. 12, p. 2300336, 2023.

[10] V. Purba, B. B. Johnson, S. Jafarpour, F. Bullo, and S. V. Dhople, "Dynamic aggregation of grid-tied three-phase inverters," *IEEE Transactions on Power Systems*, vol. 35, no. 2, pp. 1520–1530, 2020.

[11] F. Bizzarri, A. Brambilla, G. S. Gajani, and S. Banerjee, "Simulation of Real World Circuits: Extending Conventional Analysis Methods to Circuits Described by Heterogeneous Languages," *IEEE Circuits and Systems Magazine*, vol. 14, no. 4, pp. 51–70, Fourthquarter 2014.

[12] F. Bizzarri and A. Brambilla, "PAN and MPanSuite: Simulation Vehicles towards the Analysis and Design of Heterogeneous Mixed Electrical Systems," in *NGCAS*. IEEE, 2017, pp. 1–4.

[13] D. Linaro, D. del Giudice, F. Bizzarri, and A. Brambilla, "PanSuite: A free simulation environment for the analysis of hybrid electrical power systems," *Electric Power Systems Research*, vol. 212, p. 108354, 2022.

[14] W. Du, F. K. Tuffner, K. P. Schneider, R. H. Lasseter, J. Xie, Z. Chen, and B. Bhattarai, "Modeling of grid-forming and grid-following inverters for dynamic simulation of large-scale distribution systems," *IEEE Transactions on Power Delivery*, vol. 36, no. 4, pp. 2035–2045, 2021.